Inhibiting the sp2 carbon deposition by adjunction of sulphurous species in refractory ceramics subjected to CO and H2 reducing atmosphere

Joris Kadok, Nicolas Bost, Antoine Coulon, Mohamed Ramzi Ammar, Séverine Brassamin, Cécile Genevois, Auriane Etienne, Aurélien Canizares, Jacques Poirier

Version of Record: https://www.sciencedirect.com/science/article/pii/S0955221919301517
Manuscript_f9485f6335985bdc28dc853dc0c9353a

Inhibiting the sp^2 carbon deposition by adjunction of sulphurous species in refractory ceramics submitted to CO and H_2 reducing atmosphere

Joris Kadok[1], Nicolas Bost[1], Antoine Coulon[1], Mohamed-Ramzi Ammar[1], Séverine Brassamin[1], Cécile Genevois[1], Auriane Etienne[2], Aurélien Canizarès[1], and Jacques Poirier[1]*

[1]*CNRS, CEMHTI UPR3079, Université Orléans, F-45071 Orléans, France*
[2]*Normandie Univ, UNIROUEN, INSA Rouen, CNRS, Groupe de Physique des Matériaux, F-76000 Rouen, France*

Abstract

The formation of sp^2 carbon by the Boudouard reaction significantly damages the refractory ceramics. Sulphur is an efficient way to prevent the carbon deposition catalysed by Fe_3C, in the presence of H_2. Thermogravimetric analysis was carried out on Fe_2O_3 samples exposed to a CO/H_2 gas mixture at 600 °C. Solid sulphur was mixed with Fe_2O_3 powder or continually added in the form of gas into the CO/H_2 reducing gas. The samples were characterised by X-ray diffraction, Raman spectroscopy, SEM and TEM. The addition of 100 ppm of sulphur species in the gas prevents the formation of carbon. The mechanism that governs the inhibition of the reaction is proposed, in which the formation of a thin protective FeS layer (0.5-1 nm) is involved. This study paves the way to an effective solution to inhibit the sp^2 carbon deposition in the refractories by poisoning the Fe_3C catalyst with sulphur.

* Tel. [33]238255514 E-mail: jacques.poirier@univ-orleans.fr

1. Introduction

The formation of carbon from carbon monoxide decomposition, known as the Boudouard reaction $2CO \leftrightarrow CO_2 + C_{solid}$ has been studied extensively [1-14]. The reaction, preferentially catalysed by cementite formed from metallic and oxide particles [2], allows a maximum yield of the sp^2 carbon formation occurring between 500 and 600° [3]. P.L. Walker et al. have studied the effect of temperature and inlet carbon monoxide-hydrogen composition on the rate of carbon formation. These authors have shown that: "as the hydrogen content of the gas mixture is increased, the temperature at which the maximum rate of carbon deposition occurs also increases, this temperature ranging from 528 °C for a 99.2% CO-0.8% H_2 mixture to 630 °C for a 80.1% CO-19.9% H_2 mixture" [3].

The Fe_xO_y particles are transformed in the presence of CO into Fe_3C catalytic cementite by a carburation reaction, and the formation of carbon originates from a dissolution-precipitation mechanism. The carbon deposition can be explained by the formation of liquid iron/ Fe_3C droplets of nanometric size which dissolve carbon until the saturation limit. Carbon is segregated on the liquid surface droplet [14]. Among the catalysts, iron and iron oxides but also cobalt and nickel are particularly active between 350 °C to 750 °C [4].

Moreover, the addition of a tiny fraction of reducing gas H_2 is known to drastically increases the rate and the amount of carbon produced by the Boudouard reaction [2-3].

For example, Walker et al. [3] reported that 0.1 g of carbonyl iron catalyst in a 9 % H_2-91 % CO gas mixture at 600°C allows the formation of 10 g of solid carbon after 350 minutes [3].

Depending on the CO/H_2 ratio, this reaction can produce not only an amorphous or flocculent carbon but also more structurally organised carbon [5-13], such as nanotubes (CNT for Carbon Nano Tubes), nanofibres (CNF for Carbon Nano Fibres), platelets or shells.

Recently, Bost et al. have initiated fundamental studies [15-16] to understand the effect of various experimental parameters such as valence and particle size of iron oxide catalysts on the amount of carbon deposition in CO/H_2 gas mixtures and to characterise the structural organisation of sp^2 carbon. The influence of the degree of oxidation (Fe, FeO, Fe_3O_4 and Fe_2O_3) and the particle size (nanometre to millimetre size) of the Fe_xO_y catalyst particles on the carbon deposition rate was investigated using thermogravimetric analysis and Raman spectroscopy with different CO/H_2 gas ratios.

The results show that the valence of the iron is not the key point that governs the amount of carbon deposited, but the carbon formation depends on the specific surface area of the catalytic particles. When the gas is composed of 100 % CO, a well-organised sp^2 carbon in the shape of encapsulating polyaromatic shells is formed around large catalytic Fe_3C particles.

Under these conditions, the smaller the initial particle size is, the higher the carbon formation rate is due to a higher specific area which induces a higher catalytic activity of Fe_3C [15]. Hematite (ρ = 5.25 g/cm^3) is firstly reduced to maghemite (ρ= 4.86 g/cm^3) then to magnetite (ρ = 5,15 g/cm3) and finally to cementite (ρ = 7,4 g/cm3). Krause and Pötschke [14] suggest the primary recrystallization of hematite to magnetite causes an enlargement of the reactive surface. The reactions of hematite reduction which occur with volume changes are possible under CO at temperatures of about 350°C.

Under CO-H_2 atmosphere, these phase transformations result in a dramatic increase in the specific surface areas of catalytic particles. The carbon growth rate is hence faster and favours the nucleation of polyaromatic carbon nanofibres on the resulting Fe_3C particles [16].

Consequently, the surface of the iron oxides plays a major role in the kinetics of the carbon formation reaction.

These different types of carbon produced by the Boudouard reaction inspire a great interest because they exhibit multiple interesting properties, such as remarkably high Young's modulus and tensile strength for CNTs and CNFs [17-18]. Graphene nanoplatelets are known to reinforce the mechanical and electrical properties of composite materials [19].

However, the formation of large quantities of sp^2 carbon can be undesirable in some specific situations. Refractory materials, containing iron oxides as impurities of raw materials and subjected to a reducing gas, are strongly degraded due to destructive carbon deposits present in the open porosity [14].

Fig. 1 shows the degradation of refractory castable samples after a CO-test (determination of resistance to carbon monoxide), according to the European standard EN ISO 12676. Carbon deposits on iron oxide spots and thereby disintegrates the refractory material.

Figure 1. Deposits of carbon and degradation of refractory castable samples after laboratory CO-test (by courtesy of ECREF).

The CO resistance of refractories is usually improved by the choice of raw materials with a low content of iron oxide impurities and by the increase of sintering temperature. However, these solutions are not effective enough for new applications such as low-CO blast furnace process in which refractories are subjected to CO and H_2 gas.

The literature on the mechanism of metal dusting corrosion [20-22], even though it is indirectly concerned with this issue, points to possible avenues of research to prevent the formation of carbon. In a CO-H_2 atmosphere at approximately 600°C, the metal dusting phenomenon causes large deposits of fine graphitized carbon particles [23] along with the catastrophic corrosion of Fe-, Co- and Ni-based metals and alloys. The metal dusting is explained by the growth of a cementite layer at the surface of the metal by carbon transfer from $CO_{(g)}$ followed by graphite formation on the cementite. The decomposition of the cementite leads to the release of fine metal particles that will act as catalysts for further carbon formation [24]. Hydrogen increases the carbon formation rate [25]. The addition of a sulphurous gas under metal dusting conditions is well known to prevent the usual deleterious effect caused by this phenomenon on metals [24], [26-28].

Schneider *et al.*, for instance, carefully studied the influence of $H_2S(g)$ on iron under similar conditions, i.e., between 500 °C and 700 °C in a CO-H_2-H_2O-H_2S atmosphere [24], [27], [28]. These authors reveal that under such conditions, the adsorption of elemental sulphur occurs via the reaction:

$$H_2S = H_2 + S_{adsorbed}$$

Karcher *et al.* also showed that SO_2 gas inhibits the carbon deposition on an iron and steel surface [29]. Troilit or pyrrhotite crystallize at the surface of cementite. A layer of FeS is formed at the catalyst surface of the metal and acts as a H_2-CO barrier which prevents the nucleation and the growth of carbon.

The aim of the present paper is to investigate the inhibition of the sp^2 carbon formation in refractory ceramics from CO decomposition catalysed by iron oxides under the most favourable conditions of the reaction, i.e., in the presence of H_2 at 600 °C, and to describe in detail the mechanisms of carbon inhibition.

Only few research studies focus on the inhibition of the sp^2 carbon deposition in refractory ceramics submitted to CO and H_2 reducing atmosphere [3], [26], [29]. The effect of sulphur on the carbon deposition produced by the Boudouard reaction, catalysed by cementite in presence of H_2 gas, was investigated under laboratory conditions.

First, the materials and the experimental means are presented and the Boudouard reaction with or without S inhibitors is described in detail. The morphological and structural evolution

of iron carbide and carbon nanoparticles is studied. The effect of the addition of different concentrations of solid sulphur $S_{(s)}$ and sulphur dioxide SO_2 (g) that inhibits the carbon formation is quantified and a mechanism of carbon inhibition by the sulphur is proposed. Finally, this study paves the way to an effective solution to inhibit the sp^2 carbon formation by the Boudouard reaction in the refractories by poisoning the Fe_3C catalyst with sulphur.

2. Materials and methods

2.1. Materials

Iron present in refractories have two origins. The natural iron impurities of the raw materials are hematite, especially if the raw materials have been heat treated. In addition, the impurities from crushing and granulation may contain mainly iron and a smaller amount of Ni, Co and W. With regard to the damage of the refractories, hematite plays an essential role. So, Fe_2O_3 iron oxide particles were used to carry out laboratory trials. Fe_2O_3 powder with a particle size of 2.5 µm was purchased from the Sigma Aldrich Company (Table 1). The specific surface of Fe_2O_3 particles was determined for information from the N_2 adsorption isotherms at 77 K at a relative pressure (P/P_0) range of 10^{-6} to 1 atm. (Autosorb-1MP, Quantachrome) by applying the BET equation. It should be noted that the initial geometry of Fe_2O_3 particles is not an essential experimental value since this geometry changes drastically when the reactive atmosphere (CO, H_2) is present.

Solid sulphur and sulphur dioxide are used as inhibitors of the carbon deposition via the Boudouard reaction, as detailed in Table 1. The reducing gas mixture (71 % CO, 3 % CO_2, 11 % H_2, 15 % N_2), hereinafter referred to as CO/H_2 gas, was similar to the CO-H_2 recycled gas mixture in future low-CO blast furnace industrial processes, in the context of Ultra Low CO_2 Steelmaking (ULCOS) initiative. This composition of gas was previously used in the research work published in the papers [15-16]

Table 1: Origin and purity of the materials used

	Materials	Origin	Purity (wt%)	Particle size (µm)	Specific Surface (m^2/g)
Catalysts	Fe_2O_3	Sigma Aldrich	>99	2-5 [a]	8.0
Reducing gas	CO/H_2	Air Liquide	>99.9		
Sulphur dioxide	SO_2 (g)	Air Liquide	>99.9		
Solid sulphur	S	Alfa Aesar	>99,5	≤ 10 [b]	

[a]Data as provided by the Sigma-Aldrich Company, [b]Prepared by grinding in an agate mortar.

A low cement castable (Refracast LCC-80R/TS – Refratechnic) has been used to validate inhibition of carbon deposition by gaseous sulphur.

2.2. Methods

To study the effect of sulphur on the formation of carbon produced by the Boudouard reaction, Fe_2O_3 powders were mixed with S. The boiling point of sulphur being 444.6 °C, under the test conditions (600°C) the sulphur is gaseous.

Laboratory tests were also carried out with SO_2 (g) to understand the effect of gaseous sulphur on the formation of carbon produced by the Boudouard reaction. SO_2 (g) was mixed continuously with the reducing CO/H_2 gas. The SO_2 (g) quantities were controlled using valves and gas flow meters of great accuracy. H_2S (g) was not used for two reasons: firstly, to have only one hydrogen source (H_2) for a better control, and second, because SO_2 (g) is a less toxic gas than H_2S (g).

Preliminary trials were performed in a horizontal tubular furnace, composed of an alumina tube (Pyrox®/Eurotherm 902P). In order to quantify the carbon growth rate, these macroscopic measurements of carbon formation were completed by thermogravimetric analysis measurements. Thermogravimetric analyses were carried out on Fe_2O_3 samples exposed to a CO/H_2 gas mixture at 600 °C. Measurements of Fe_2O_3 mass variation were performed using a thermobalance from NETZSCH STA 409C/CD coupled with a QMS 403/5 Skimmer. The reproducibility of the TGA instrument, given by NETZSCH, is ± 0.1 %. Fe_2O_3 samples of approximately 30 mg were placed in an alumina crucible and were heated at 600 °C with a rate of 10 °C·min^{-1} under 100 ml·min^{-1} of an Ar inert gas prior to being exposed to a reducing CO/H_2 gas (100 ml·min^{-1}).

The structural organisation of samples and the kinetics of carbon formation were determined by X-ray diffraction and Raman spectroscopy.

The crystalline phases were analysed with powder X-ray diffraction (PXRD) using a Bruker D8 A25 diffractometer (Bragg-Brentano geometry θ-θ) equipped with a LynxEye XE detector and using the Cu K_α radiation (λ = 1.5418 Å). Each scan was recorded in a 2θ range from 20 to 60° with a step size of 0.016 at 10 s per step.

Raman spectroscopy was performed using a T64000 Jobin-Yvon multichannel spectrometer equipped with an Ar-Kr laser source, aBX41 Olympus microscope and a liquid nitrogen-cooled CCD detector. The spectra were collected in a backscattering geometry under a

microscope (×20 long working distance objective) using the 514.5 nm wavelength (2.41 eV; 3 mW of laser power), a 600 groves·nm^{-1} grating giving a spectral resolution of 3 cm^{-1} in the 1000-2000 cm^{-1} wavenumber range. Heating the sample was achieved using a TS1500 Linkam device (Tadworth, U.K.) [17]. The TS1500 heating stage was connected to a pressurized gas cylinder using inox tubes. The same temperature program was used for Raman spectroscopy and for TGA (10°C·min^{-1} until 600°C). The carbon deposit was analysed, *in situ*, at high temperature for 240 minutes, with a Raman acquisition time of one minute.

After the experiments, the samples were also characterised by microscopic observations. Scanning electron microscopy (SEM) was carried out using a Hitachi S4500 FEG on polished sections. High resolution transmission electron microscopy (HRTEM) was also used to characterise the nanostructure of the different samples. HRTEM images were collected using a Philips CM20 microscope. Elemental compositions and STEM images were carried out on a JEOL ARM200F (JEOL Ltd.) cold FEG operating at 120 kV and equipped with a TEM/STEM double spherical aberration (Cs) correctors. Scanning transmission electron microscopy - high angle annular dark field (STEM-HAADF) images were acquired in the angular range of 50-180 mrad with an 8 cm camera length and a 0.1 nm probe size. Elemental composition line scans were performed by STEM-EDS using a JEOL EDS (Energy Dispersive Spectroscopy) system and a 0.13 nm probe size. Samples were prepared by dispersing a small amount of the material in ethanol using an ultrasound bath. A drop of the solution was deposited onto a holey carbon-coated copper grid.

3. Results

3.1.Effect of sulphur on the amount of carbon produced by the Boudouard reaction

This section focusses on preventing the formation of carbon from CO decomposition catalysed by iron oxides, by adding sulphur, in a solid or gaseous form. Laboratory experiments were carried out to understand the relevant parameters taking place in the carbon formation and to examine the effect of the S addition on the C deposition by the Boudouard reaction. The experiments were carried out under optimal conditions for the formation of carbon, i.e., with Fe_2O_3 at 600 °C under a gas mixture (71 % CO, 3 % CO_2, 11 % H_2, 15 % N_2).

3.1.1. Preliminary experiments

In order to ascertain the beneficial effect of sulphur addition on the inhibition of carbon deposition, preliminary macroscopic tests were carried out on a larger scale of observation. Fe_2O_3 powders were mixed with pure sulphur. The samples (1 g) were placed in an alumina basket and then heated to 600°C under air at a rate of 10°C·min^{-1} prior to being exposed to the CO/H_2 gas with a 28 L·h^{-1} flow rate, for one hour.

Figure 2 shows a photograph of the samples. The 100 wt.% Fe_2O_3 sample shows a significant carbon deposition with a morphology of "popcorn" in accordance with the literature [15]. The samples containing sulphur have only a change in colour (Figure 2 c-d). The black colour is caused by the reduction of hematite to cementite. It can be shown that carbon formation is inhibited if solid sulphur is part of the starting composition.

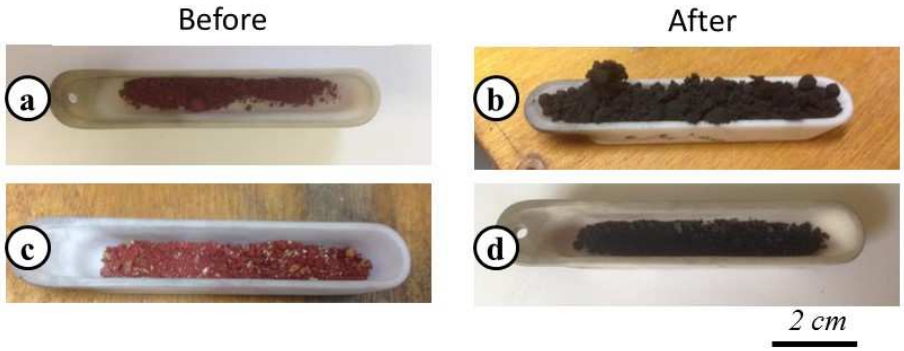

Figure 2- Photography of samples before and after a treatment under a gas flux of 28 L·h^{-1} of a CO/H_2 reducing gas, at 600°C, for one hour *(Pyrox®/Eurotherm 902P furnace)*. a, b - 100 % Fe_2O_3; c, d-70 % Fe_2O_3 + 30 % S

A Fe_2O_3 bulk sample (0.66g) was heated to 600°C at a rate of 10°C·min^{-1} under pure SO_2 (g) with a 20 L·h^{-1} flow rate prior to being exposed to the CO/H_2 gas with a 25 L·h^{-1} flow rate, for one hour. After experiment, no carbon deposits are detected.

SEM micrograph shows a layer at the surface of the sample (Figure 3-a). The initial sample is partially fragmented due to the reduction of the iron oxide sample by H_2 and CO (Figure 3-b). EDS analysis reveals also the presence of FeS with a concentration gradient of S about 4 mm thick (Figure 3-c, d, e).

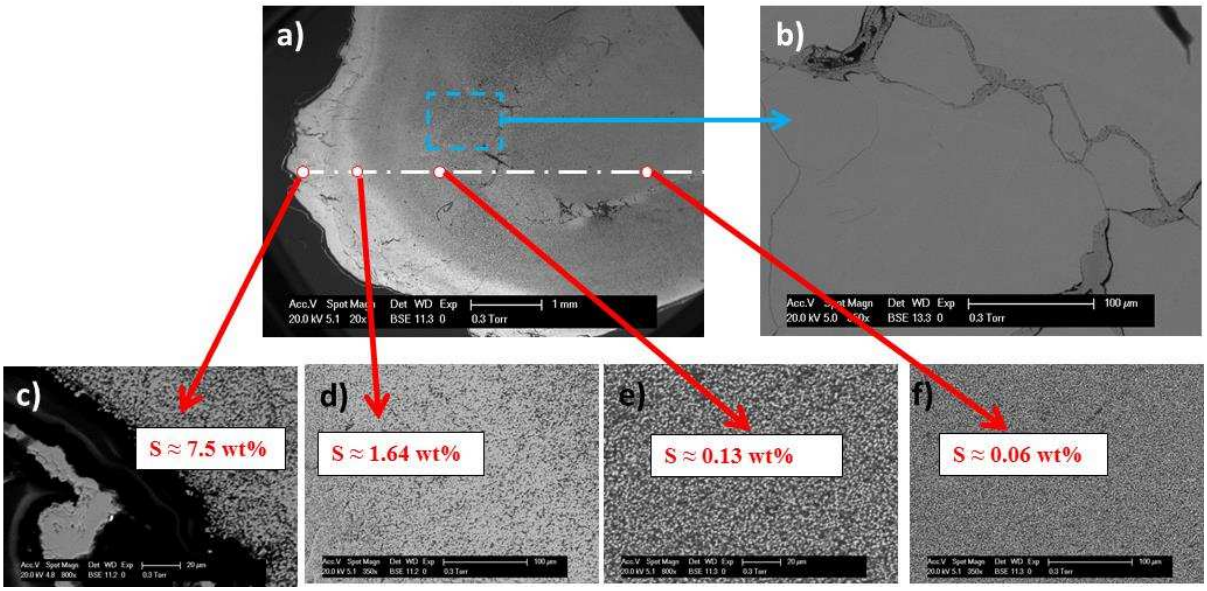

Figure 3- Scanning electron micrograph of Fe_2O_3 bulk sample after experiment

a) and b) Overview and detail of the sample

c),d),e),f) EDS analysis of S

These preliminary tests show that sulphur and sulphur dioxide inhibit carbon deposition. In contact with SO_2 (g), FeS is formed on the surface of the Fe_2O_3 particles and the carbon deposit is not formed. SO_2 gas seems to have a delayed effect on the carbon formation.

Sulphur obviously poisons cementite, which no longer acts as a catalyst. As a result, CO is more stable than C + CO_2, as it should be under the given ambient conditions.

The next step is to quantify the effect of inhibiting sulphur on the carbon deposition produced by the Boudouard reaction.

3.1.2. Thermogravimetry analysis

TGA experiments were performed to quantify the effect of inhibiting sulphur on carbon growth rate as a function of the S amount in the various solid or gaseous mixtures.

TGA experiments with solid sulphur

Fe_2O_3 powder was mixed with sulphur in different amounts: 1, 5, 10 and 30 wt.% S. Figure 4 shows the mass variation of samples in time (full lines) obtained from thermogravimetric measurements as well as the variation in the temperature (dashed lines) as a function of time. The TGA results of mixtures (Fe_2O_3+S) are compared to an experiment without S addition.

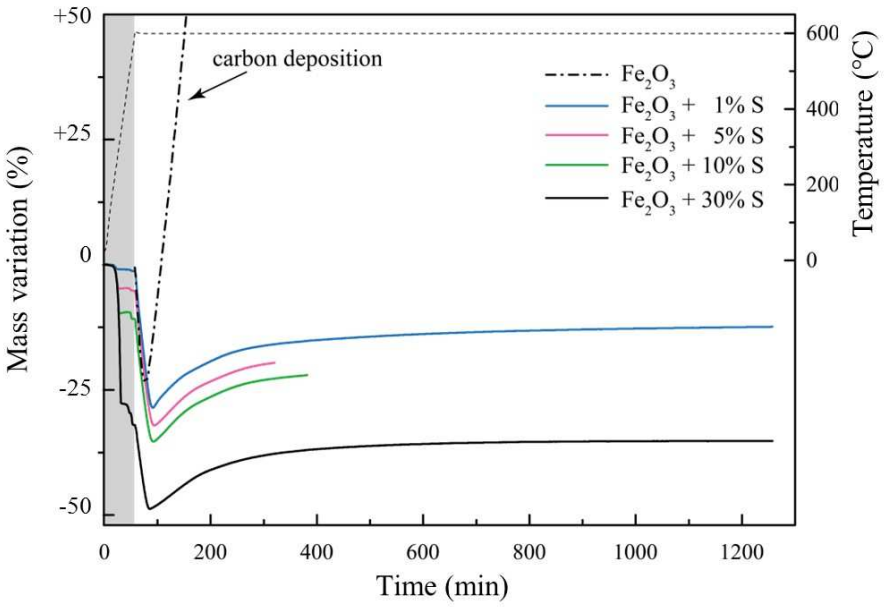

Figure 4- TGA curves of the samples exposed to the CO/H_2 reducing gas mixture at 600 °C - Mixture of Fe_2O_3 powders and pure S (1, 5, 10 and 30 wt.%)
The grey area shows the heating stage to 600°C under an inert gas (Ar)

Several chemical reactions with gain and loss of mass occur simultaneously. During heating at a rate of 10°C.min^{-1}, under an inert atmosphere (100 ml·min^{-1} Ar), Fe_2O_3 + S mixtures have a mass loss associated with sulphur vaporisation at 440 °C, proportional to the amount of the introduced S (Figure 4). The mass balance of the TGA experiments performed with S + Fe_2O_3 samples at the temperature of sulphur vaporisation (440°C) and prior to the injection of CO/H_2 gas (600°C) is presented in the table 2.

Table 2- Mass balance of the TGA experiments

Initial S (wt%)	Mass loss: Δm (%) at 440°C – 44 min at S vaporisation temperature	Mass loss Δm (%) at 600°C – 60 min at injection of CO/H_2 gas
1	0,92	1.03
5	4.55	5.36
10	9.25	10.11
30	27.97	29.99

Almost all the sulphur volatilises prior the injection of the CO/H_2 gas. The amount of sulphur adsorbed on the surface of the Fe_2O_3 particles is extremely small. The FeS layer is formed at the volatilization temperature of sulphur, prior the CO / H_2 injection. Higher concentrations of solid precursor sulphur are not beneficial for the formation of the FeS layer. The stability over time of FeS will be discussed in the paragraph: “Retarding effect of sulphur on the carbon deposition”.

After 60 minutes, the injection of Ar gas is stopped and CO/H_2 reducing gas is introduced continuously (100 $ml \cdot min^{-1}$). A weight loss approximately of 25 wt.% is observed due to the chemical reduction of the iron oxides by hydrogen and carbon monoxide (the theoretical weight loss is 30.06 %), as previously explained in literature [15]. The Fe_2O_3 reference sample shows a very important carbon deposit. The samples containing sulphur have a significantly lower weight gain, similar for all the samples (approximately 12.5 wt.%) that stabilizes after 400 minutes.

TGA experiments with gaseous sulphur compounds

A continuous introduction of gaseous sulphur dioxide SO_2 in CO / H_2 mixture has many advantages compared to a solid sulphur addition. Indeed, the solid sulphur volatilizes at 440 °C and the amount of sulphur adsorbed on the surface of the particles is extremely low. The SO_2 (g) leads to a more sustainable amount of sulphur and thus more efficient inhibition of carbon formation in time.

The experiments were carried out with Fe_2O_3 at 600 °C under a mixture of CO/H_2 reducing gas containing SO_2 (g). The gas flow rate was 100 $ml \cdot min^{-1}$.

A mass balance in the following experimental conditions (180 min at 600 °C under a mixture of CO / H_2 gas containing 1000 ppm of SO_2 (g) with a gas flow rate of 100 $ml.min^{-1}$) show that ratio S injected / Fe_2O_3 is equal to 3.4 wt. %.

Figure 5 shows the TGA results (mass variation as a function of time) for SO_2 (g) content equal to 1, 10, 50, 100 and 1000 ppm, and the results are compared to an experiment without SO_2 (g) addition. Once the gas mixture was injected, all the samples underwent a similar mass loss for approximately 20 minutes, due to the Fe_2O_3 chemical reduction into pure iron prior to its carburation in iron carbide [15]. For the samples exposed to a gas mixture containing 1 to 10 ppm of SO_2 (g), a dramatic mass gain is observed due to carbon formation, roughly similar to what could be found without SO_2 (g). Table 3 indicates the linear carbon growth rate in $mg \cdot h^{-1}$ for different experimental conditions. SO_2 content (1 and 10 ppm) is obviously not sufficient to lower significantly the carbon formation. When 50 ppm of SO_2 was injected, a lower mass gain was observed, and the carbon growth rate was decreased by a factor of 5 in comparison with the experiment without SO_2. For 100 ppm and 1000 ppm of SO_2, the carbon growth rate values were decreased by a factor of 70. However, a slightly higher mass gain is observed for the sample with 100 ppm of SO_2 in comparison with 1000 ppm.

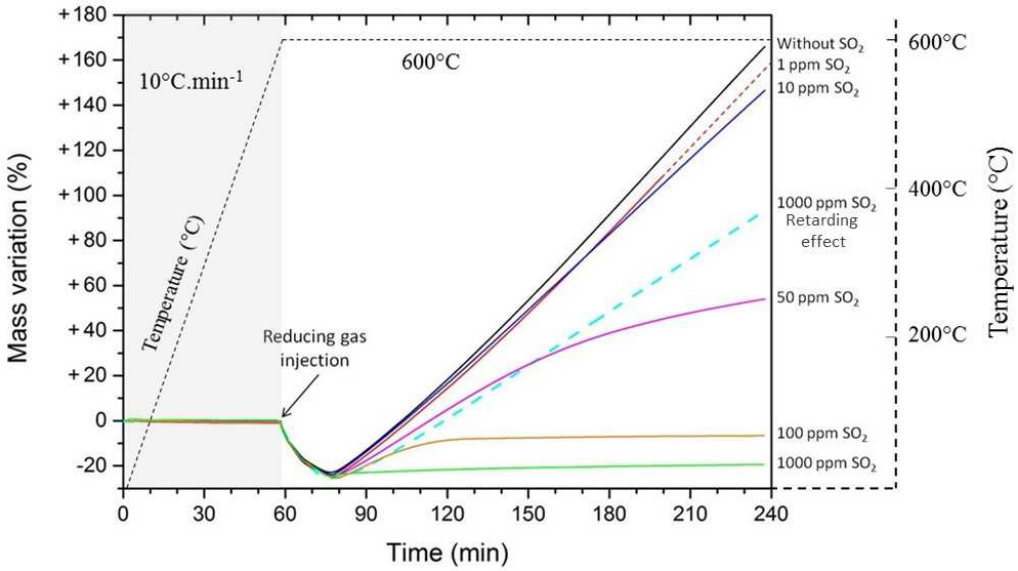

Figure 5- TGA curves of the Fe_2O_3 samples exposed to the reducing gas mixture containing small fractions of SO_2 (g) at 600 °C (continuous curves). The results from the retarding effect of SO_2 (g) experiment (see paragraph Retarding effect of sulphur on the carbon deposition) are also given for comparison (bold dashed curve).
The grey area shows the heating stage to 600°C under an inert gas (Ar)

Table 3- Linear carbon growth rate for TGA experiments. The initial sample masses were approximately 30 mg of Fe_2O_3.

SO_2 Content (ppm)	Carbon Growth Rate ($mg \cdot h^{-1}$)
0	21.6
1	21.0
10	19.5
1000	0.3

*The carbon growth rate was not determined for 50 and 100 ppm SO_2 content, as the curves were not linear.

Retarding effect of sulphur on the carbon deposition

To determine if the initial introduction of SO_2 gas has a retarding effect on the carbon formation produced by the Boudouard reaction, a TGA experiment was carried out in two steps:

1. The Fe_2O_3 sample was exposed to the N_2 gas (100 $ml \cdot min^{-1}$) containing 1000 ppm of SO_2 (g), over 3 hours at 600 °C. In that case, the sulphur is adsorbed on the surface of the iron oxide sample.

2. Then, the composition of the gas is modified. The initial gas, N_2 containing 1000 ppm of SO_2 (g), is replaced by the CO/H_2 gas (100 ml·min^{-1}) without SO_2(g) additions for 3 hours in addition at 600°C.

The resulting curve is shown in Figure 5 (bold dashed blue curve, superimposed on the other curves, on the same graph). A retarding effect of sulphur is observed. The carbon growth rate for this experiment is 16.4 mg·h^{-1}, which is significantly lower than for the experiment without SO_2 (21.6 mg·h^{-1}) but higher than for the experiment under CO/H_2 reducing gas containing 1000 ppm SO_2 (0.3 mg·h^{-1}), which shows a significant inhibition but not a total prevention of the carbon formation. Moreover, the temporary exposition to 1000 ppm of SO_2 had a lesser effect (a few hours) compared to a continuous exposition of SO_2 (g) with a lower content (100 ppm). The chemisorption of SO_2(g), reduced to S on the surface of Fe_2O_3 particles is probably at the origin of the prevention of the carbon formation. Otherwise, the elemental physisorbed sulphur would evaporate immediately because its boiling temperature (444 °C) is below the temperature of experiment. The sulphur species, which are retained in the deeper sections of the Fe_2O_3 catalyst, diffuse slowly up to the surface could thus explain the observed effect. At the microscopic scale, this mechanism is complex. It will be described in detail in a subsequent publication. The affinity of sulphur to iron being higher than the affinity of oxygen to sulphur, a sulphur rich layer formed at the surface of the initial Fe_2O_3 particles. The chemical reaction Fe + S ➔ FeS is an exothermic reaction: $\Delta H°_{FeS}$ = -102 KJ/mole. FeS limits the nucleation and growth of the sp^2 carbon nanotubes (nucleation which requires the formation of liquid / iron / iron carbide droplets). Sulphur effectively delays carbon deposition but does not suppress it. FeS has a limited effect in time (a few hours) and is therefore not stable. The reason for this instability is an important point that is discussed in paragraph 4.

So, the mechanism of sulphur chemisorption does not appear to be sustainable and hence requires a continuous SO_2 (g) exposition. From TGA experiments, it is shown that 1% S_{solid} or 100 ppm SO_2 (g) are sufficient to inhibit carbon formation. The structural and morphological evolution of the samples is presented in the following paragraph.

3.2.Structural evolution of samples and kinetics of carbon formation

The evolution of crystalline phases of each sample, after the TGA experiments, was characterised by powder X-ray diffraction. PXRD patterns of the samples exposed to 0, 10, 50, 100 and 1000 ppm of SO_2 under TGA are presented in Figure 6.a.

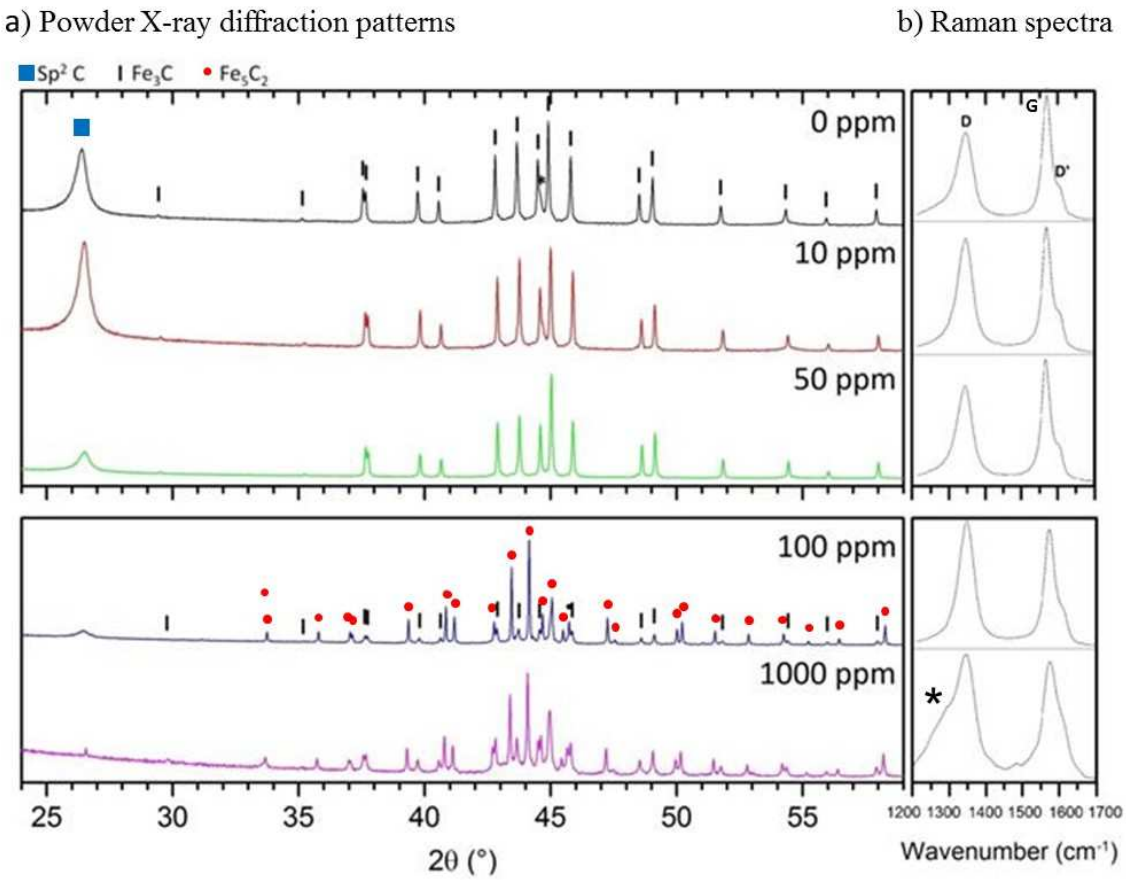

Figure 6- a) Powder X-ray diffraction patterns of the samples obtained after TGA experiments under 0, 10, 50, 100 and 1000 ppm of SO_2. Fe_3C and sp^2 carbon are found in each pattern whereas the Fe_5C_2 carbide is found only under 100 and 1000 ppm of SO_2. The 0, 10 and 50 ppm patterns are normalized with the highest Bragg reflection of the Fe_3C phase (031) and the 100 and 1000 ppm patterns with the highest Bragg reflection of the Fe_5C_2 phase (510).
b) Raman spectra of the carbon obtained after TGA experiments under 0, 10, 50, 100 and 1000 ppm of SO_2. These spectra contain three main bands: G band and the defect-induced D and D' bands
* *Fe_2O_3 magnon peak*

From 0 to 50 ppm of SO_2, PXRD diffractograms exhibit reflections that can be all indexed with sp^2 carbon (C – JCDPS 01-089-8487) and cementite (Fe_3C - JCDPS file 01-079-4902). For 100 and 1000 ppm of SO_2, the Hägg carbide (Fe_5C_2- JCDPS 01-076-3842) is also observed. Compared to the cementite which crystallizes in an orthorhombic lattice with parameters a = 5.0807(2) Å, b = 6.753(1) Å and c = 5.5152(3) Å (Pearson symbol $oP16$) [30], the Hägg carbide crystallizes in a monoclinic lattice with parameters a = 11.56953(7) Å, b = 5.45252(3) Å, c = 5.06043(3) Å and β = 97.7308(4) Å (Pearson symbol $mS28$) [31]. The crystal structure of these two compounds is similar in the sense that they can be described by a stacking of identical Fe and Fe-C atomic planes. However, the two compounds differ in the stacking order and orientations of those planes. The presence of these two phases in the PXRD patterns is in accordance with the literature. Schneider *et al.* reported that the

increasing contents of H_2S for pure iron samples under metal dusting conditions (CO + H_2 at 500 °C) favours the formation of this Fe_5C_2 compound [24]. On every PXRD pattern, the (002) carbon reflexion is broad shaped, indicating an imperfectly crystallized carbon. Its intensity tends to decrease with the increase of the SO_2 content. These results are consistent with TGA experiments where the carbon formation was decreasing with the increasing SO_2 (g) content. Iron sulphide phases are not detected on PXRD diffractograms.

In addition to X-ray diffraction, Raman spectroscopy was performed to study the structural evolution of carbon deposits, for iron oxide samples exposed to 0, 10, 50, 100 and 1000 ppm of SO_2 (Figure 6.b)

Raman spectroscopy is a very sensitive characterisation method that reveals the presence of carbon as well as its structural state from perfectly crystalline to amorphous [32-33].

The Raman spectra of the sp^2 carbon contain three main bands that range from 1000 to 2000 cm^{-1}:

- G band, located at approximately 1580 cm^{-1} when recorded at room temperature, that corresponds to the in-plane bond stretching of carbon atoms (E_{2g} symmetry)
- Two defect bands (D: ≃ 1250-1400 cm^{-1} and D': ≃ 1600-1630 cm^{-1}) originating from a peculiar interaction between electrons and phonons due to defects in the crystal structure [34].

The I_D/I_G intensity ratio of the D and G bands and the G band full width at half maximum (FWHM) are commonly used to characterise the disorder of carbon-based materials [32], [35-39].

In a previous publication [16], Bost *et al.* have shown that the Raman spectrum of sp^2 carbon produced by the Boudouard reaction catalysed by iron oxide, in a pure CO atmosphere without hydrogen, exhibits only a sharp G band. The absence of the defect-induced D band suggests a high degree of crystallinity with important coherent domain diameters of the resulting carbon, similar to what could be found for graphite. In contrast, the sp^2 carbon produced in a CO/H_2 gas mixture turns out to be in the form of nanofibres, and the corresponding Raman spectrum exhibits a pronounced D band activated by the boundaries that constitute these nanofibres.

When 0, 10 and 50 ppm of SO_2 is used, Raman spectra (Figure 6.b), characterised by a pronounced D band, display similar structural organisation of the nanofibres produced. However, the Raman spectra of the samples exposed to 100 and particularly 1000 ppm of SO_2 exhibit some differences. The FWHM of the G band is relatively wider for these samples,

particularly the sample exposed to 1000 ppm of SO_2. This is a signature of the production of more disordered carbons or nanofibres with lower coherent domain diameters. Basically, *ex situ* Raman spectroscopy cannot be used here to provide quantitative information about the amount of the sp^2 carbon produced owing to the absorbent character of this material to the visible light and therefore the penetration depth of the excitation laser used. In fact, the band located at approximately 1310 cm^{-1} and appears as a shoulder of the D band is attributed to magnon scattering mode and its presence is an indirect evidence of the small amount of the produced carbon, especially for the samples exposed to 1000 ppm of SO_2. PXRD is completely silent about this where no (002) carbon reflection is observed, which shows the high sensitivity of Raman spectroscopy in probing sp^2 carbon materials and the complementarity of the characterisation techniques used.

In situ Raman spectroscopy, at 600°C, has also been carried out to determine the kinetics of the carbon formation (Figure 7). Approximately 1 mg of Fe_2O_3 was first heated to 600 °C under N_2 prior to being exposed to the reducing gas mixture with or without the SO_2 containing gas ($\simeq$ 24 $L \cdot h^{-1}$). Raman spectra were acquired every minute during the experiments.

The intensity of the G band (in arbitrary units) versus time is plotted for the *in situ* Raman experiments without SO_2 and with 1000 ppm of SO_2, as shown in Figure 7.

Considering the fact that the G band is proportional to the amount of the carbon exposed to the excitation laser, two pieces of information can then be extracted here.

1. The introduction of 1000 ppm SO_2 in the gas mixture clearly has a delaying effect in the formation of carbon since this latter starts to be probed after more than 1 hour (Figure 7.b), while the detection of carbon was immediate in the absence of SO_2 (Figure 7-a).
2. The formation of carbon without SO_2 is so important that the intensity I_G starts to decrease after 90 minutes (Figure 7.a) due to the laser defocusing. In Figure 7.b, the intensity I_G remains relatively constant without decreasing and is also evidence of a tiny amount of carbon without defocusing the excitation laser.

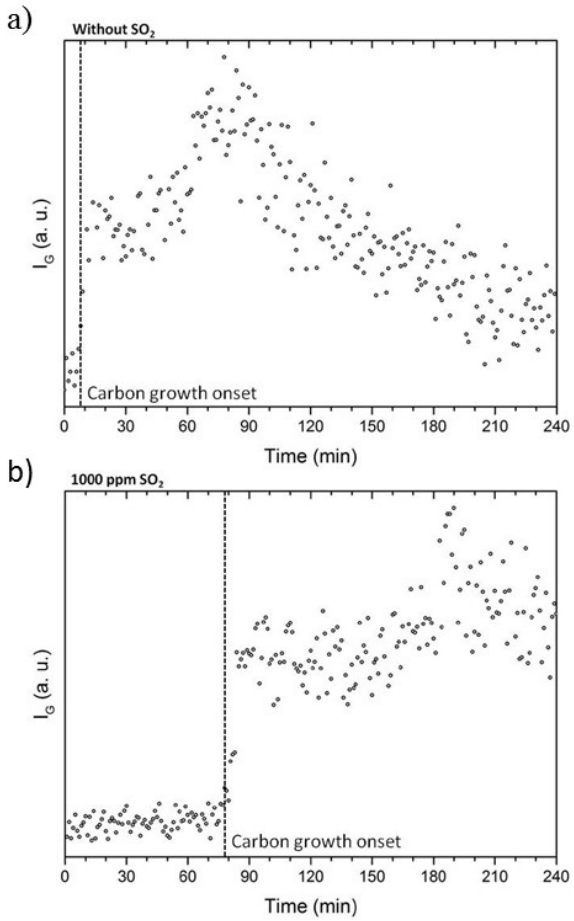

Figure 7- Intensity of the G band versus time for the *in situ* Raman experiments (at a temperature of 600°C, under CO/H_2 gas) a-without SO_2, b- with 1000 ppm of SO_2.

Considering all the experimental results (TGA, XRD and Raman spectroscopy), we can conclude that with the addition of increasing SO_2 quantities in the gas mixture (> 100 ppm), the carbon formation is significantly lowered and delayed, according to a mechanism that will be proposed in the discussion section. The effect of the Fe_3C catalyst is inhibited. However, the carbon formation is not completely prevented.

3.3.Morphological and elemental characterization of samples

To better understand the effect of sulphur on the inhibition of the carbon produced by the Boudouard reaction catalysed by Fe_2O_3, the samples were observed after TGA experiments by scanning electron microscopy (SEM) and high-resolution transmission electron microscopy (HRTEM).

Figure 8 shows typical SEM micrographs of the samples obtained in back scattering electron mode, before (a) and after (b and c) the thermobalance experiment using CO/H_2 gas without SO_2(g) addition. Before the experiment (Fig.8-a), the Fe_2O_3 particles are approximately 5 µm in diameter with a very angular aspect. After experiment (Fig. 8-b and c), the sample exhibits a dense population of particles, appearing brighter and measuring less than 0.5 µm in diameter. Considering the initial size of the Fe_2O_3 particles (2 - 5 µm), the particles were decreased in size during the experiments by the phase transformations of hematite (chemical reduction of Fe_2O_3 into Fe_3C with volumes changes and mineral recrystallizations), as previously explained [14,15].

EDS analysis systematically reveals the large presence of iron and carbon elements. The resulting material turns out to be a mixture of sp^2 carbon and iron carbide particles, as revealed by PXRD. This mixture contains a large quantity of sp^2 carbon, according to TGA and Raman spectroscopy results. The sp^2 carbon is in the form of nanofibres observed as dark phase in SEM images.

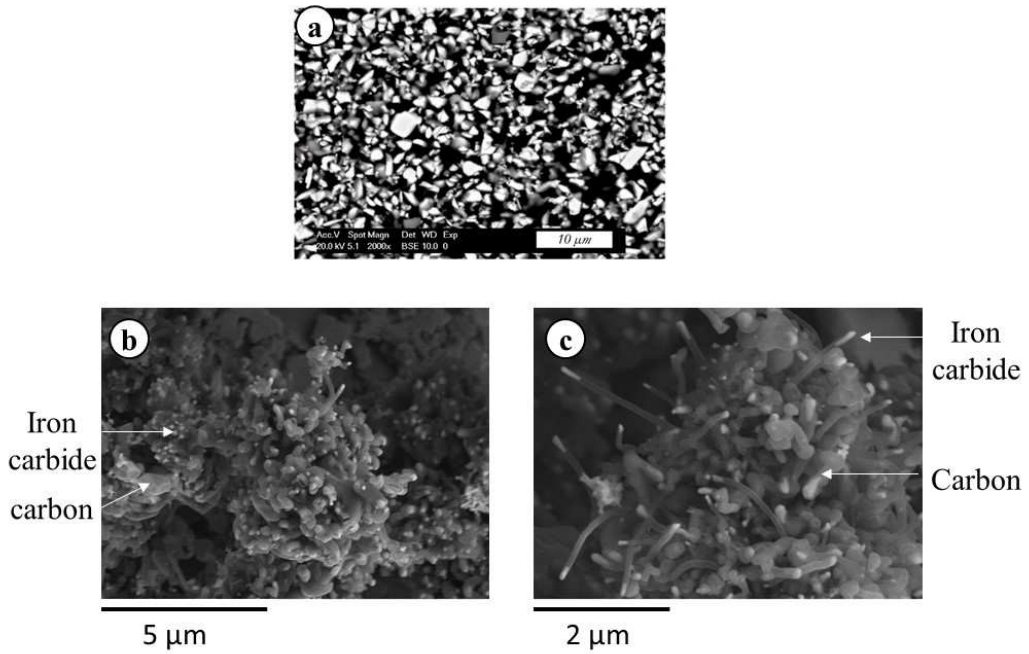

Figure 8- Scanning electron micrographs of the samples. The powder was deposited on a substrate.
a) Initial Fe_2O_3 sample prior the thermobalance experiment, at 20 kV.
b) and c) Sample after the thermobalance experiment using CO/H_2 gas without SO_2(g) addition
Images were taken at 15 kV in back-scattered electron mode (BSE)

Figure 9 shows typical SEM micrographs of the samples after the thermobalance experiment using CO/H_2 gas with SO_2(g) addition.

The sample exposed to 1000 ppm of SO_2 (g) exhibits a quite different morphology. The particles sizes do not seem to have been reduced or have been reduced to a lesser extent. EDS

analysis revealed very weak traces of sulphur, but its presence is not sufficient to precisely determine its composition and its location. As already asserted with Raman spectroscopy, a pure carbon phase, which should be present in this sample, is not observed on the micrographs because of its very small quantity. PXRD patterns revealed the presence of iron carbide particles such as Fe_3C and/or Fe_5C_2 particles (Fig.6)

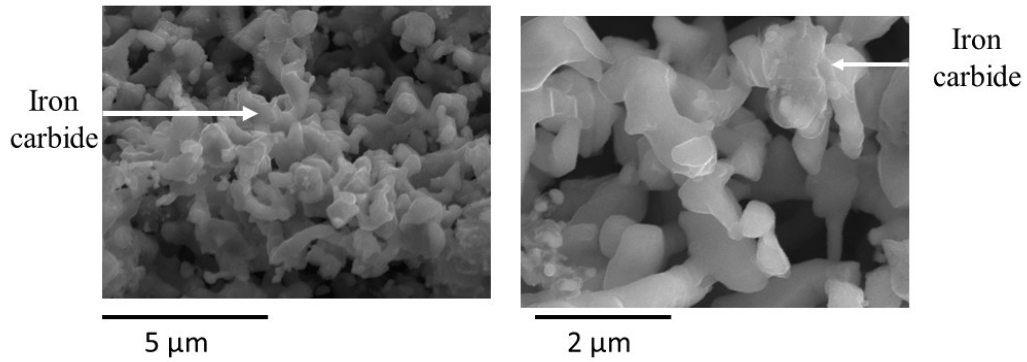

Figure 9- Scanning electron micrographs of the samples after TGA experiments using CO/H_2 gas with 1000 ppm SO_2 (g). Images were taken at 15 kV in back-scattered electron mode (BSE)

TEM micrographs of the samples not exposed to SO_2 show the presence of iron carbide (cementite) particles with a reduced size compared to the initial particle size (Figure 10.a).
The rounded shape of these particles may suggest a molten state, as previously explained by Krause and Pötschke [14]: "a prerequisite of carbon growth is the formation of liquid iron/carbide raw droplets which absorb carbon until the saturation limit; otherwise carbon deposit will not take place". A part of the carbon forms nanofibres growing from Fe_3C particles. These carbon fibres are composed of polyaromatic layers surrounding an amorphous core (see Figures 10.b and 10.c). Other Fe_3C particles without filamentous carbon are enclosed by a graphitized carbon shell (not shown on this micrograph).

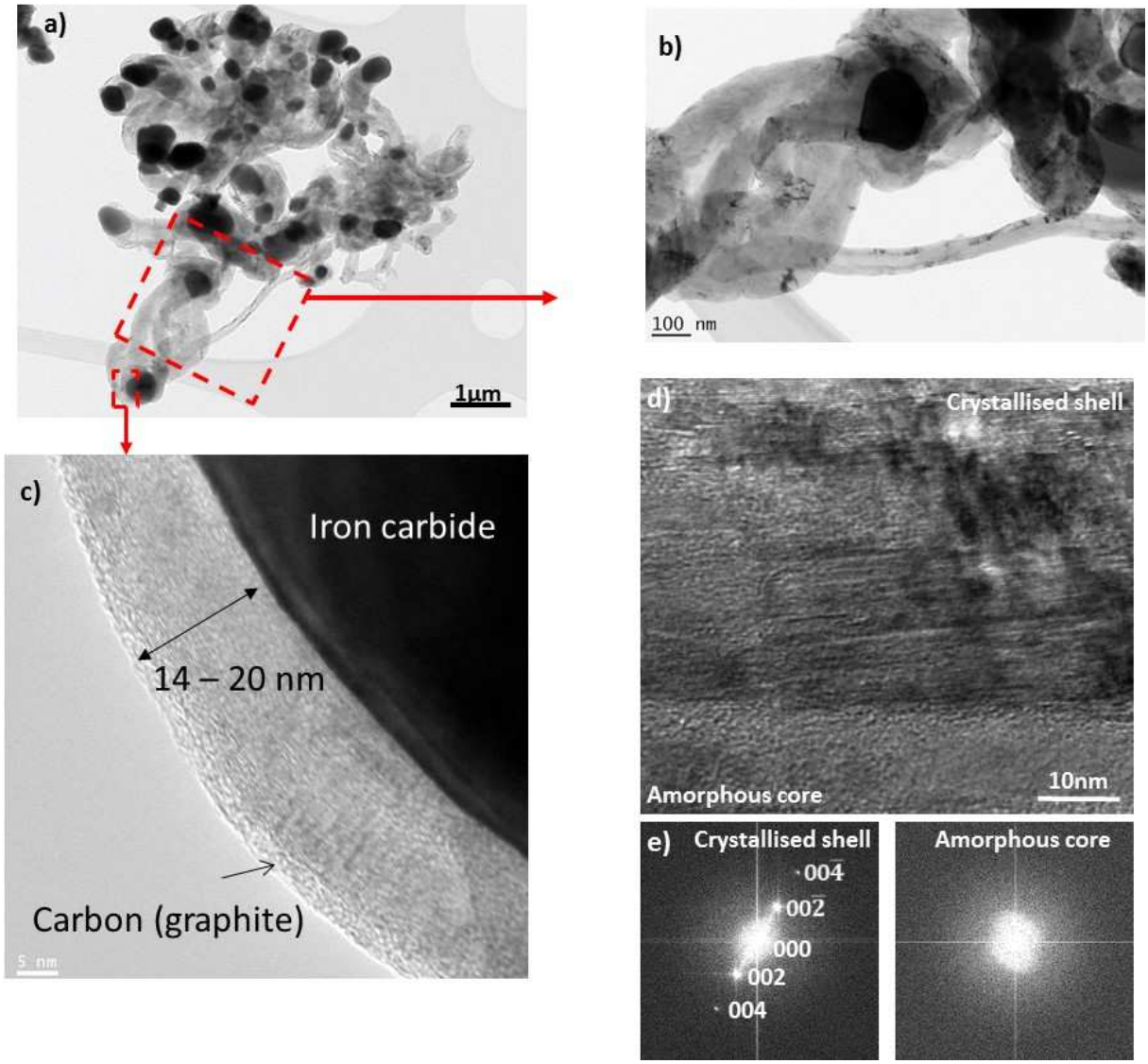

Figure 10- Transmission electron micrographs of the sample after TGA experiments without SO_2.
a), b), c) Overview and details of the sample
d) HRTEM micrograph showing details of the nanofibre.
e) Fast Fourier Transform (FFT) from the graphitized carbon located on the external layer (left panel) and from the amorphous core of the nanofibre (right panel).

A typical TEM micrograph for the sample exposed to 1000 ppm of SO_2 (g) is presented in Figure 11.a. The TEM observations, similar to SEM observations, are based on the naturally cooled samples at room temperature. Consequently, some differences could exist compared to the same samples at the temperature of experiment (600°C). At high temperature, the nanometre-sized particles are likely to be in a fluid-like state, which could favour the atomic exchanges. The state of the particles could also explain the round shapes of the particles observed. No filamentous carbon is observed on the micrograph, and the iron carbide particles are systematically covered by a nanometre-sized thick shell (Figure 11.c). High-resolution STEM-HAADF images representative of the sample show a two-layered shell (see Figure

11.b and 11.d). For STEM-HAADF images, the intensity is proportional to the density of the sample and the atomic number of the element (proportional to $Z^{1.7}$). Consequently, and contrary to the previous TEM images, the iron carbide particles appear with a brighter contrast than the carbon particles. The inner layer is very thin (0.5 - 1 nm) and seems to be composed of lighter elements compared to the outer layer (3 - 5 nm), which appears brighter. Atomic resolution STEM-HAADF images show that the particle and the outer layer are crystallized but without an apparent orientation relationship (see Figure 11.d). Such observation is, however, not as clear for the inner layer where it is not possible to distinguish the atoms. Occasionally, the inner layer does not thoroughly surround the iron carbide. In such a case, the outer layer is absent (see Figure 11.e).

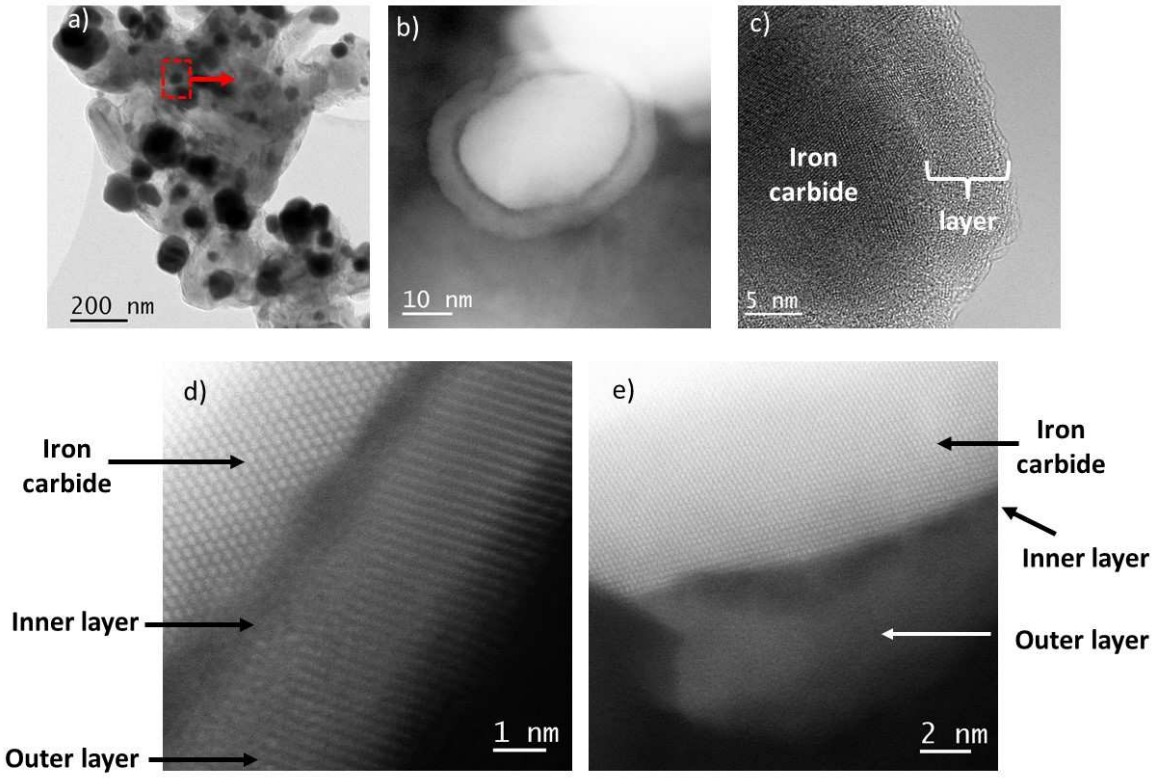

Figure 11- Micrographs of the sample after TGA experiments exposed to 1000 ppm of SO_2 (g).
a), c) TEM image representative of the sample.
b), d), e) high-resolution HAADF-STEM images of a particle surrounded by a two-layer shell.

To determine the evolution of the chemical composition, a 20-points EDS line scan has been performed with a 0.13 nm probe size through the three different domains: iron carbide particle, inner layer and outer layer (see Figure 12).

However, due to the spherical shape of the iron carbide particle, both layers, inner and outer, present all around this particle contribute slightly to modifying the composition of the iron

carbide particle measured. Likewise, the composition found for the inner layer is largely altered by the presence of the outer layer due to its subnanometre-size. The compositions given at the boundaries between the two layers should be taken with the greatest care.

According to the result of the analysis, iron is present in the three domains. Iron is more concentrated in the particle, associated with carbon. The ratio (% at) of approximately 3:1 between these two elements indicates that the particle is composed of iron carbides, Fe_3C and/or Fe_5C_2, as expected. The outer layer composition is not biased by the other domains and seems to contain the three elements: iron, oxygen and carbon, which would suggest the presence of an iron oxide along with an iron carbide and/or free carbon. The composition of the inner layer is more delicate to interpret due to its very thinness (0.5 - 1 nm) and the large contribution of the outer layer co-probing. Nevertheless, this inner layer is the domain richest in sulphur with a rather high content of iron, which suggests the formation of an iron sulphide such as FeS, as asserted by the preliminary experiments (see paragraph 3.1.1) and a previous study [24].

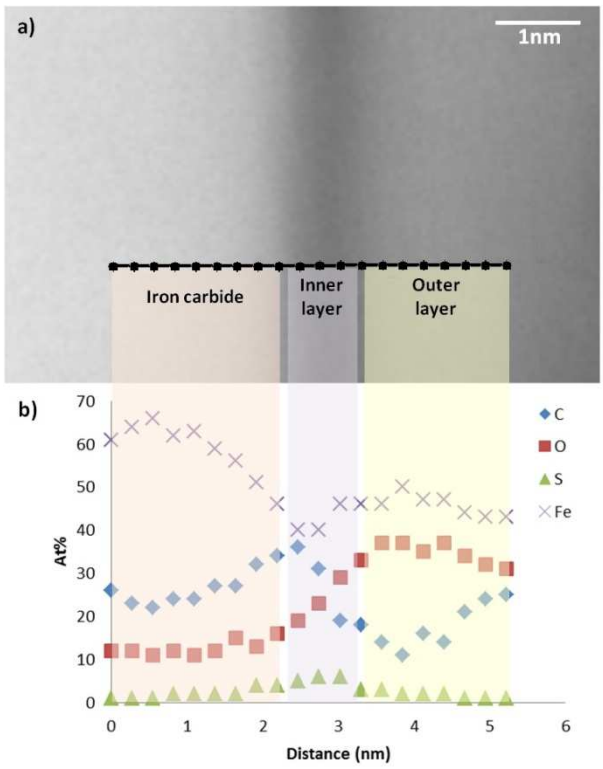

Figure 12- a) STEM-HAADF micrograph and b) composition profile (% at) through the iron carbide particle, the inner layer and the outer layer.

4. Discussion

From the experimental results and the literature, a mechanism that governs the inhibition of carbon deposition by the Boudouard reaction catalysed by cementite is proposed.

Under CO/H_2 gas without sulphur, the iron oxide particles are chemically reduced by hydrogen and CO. The iron oxide particles are converted to Fe_3C iron carbide. Liquid iron/ carbides droplets are formed which dissolve carbon until the limit of carbon saturation and favour the nucleation and the growth of nanocarbon fibres [15]. Figure 13.a summarizes the mechanism of carbon formation by the Boudouard reaction, catalysed by cementite.

With $SO_2(g)$ additions, under CO/H_2 gas, the carbon deposition by the Boudouard reaction is strongly retarded. The effect of sulphur could be explained by a multistep mechanism.

- **Reduction of SO_2 to H_2S by CO/H_2 gas**

For high H_2/SO_2 ratios, the two species H_2 and SO_2 are known to react together to form H_2S. Tai Feng *et al*. have studied the reduction of $SO_2(g)$ to elemental sulphur with H_2 and mixed H_2/CO gas [41]. Thermodynamic equilibrium calculations using the equilibrium module of the thermodynamic software Factsage 6.4 and experiments were carried out on a H_2-CO-SO_2 system and the temperature effects and H_2/SO_2 ratio were evaluated.

When the H_2/SO_2 ratio was greater than three, which is the case in our experiments, the thermodynamic calculations and the laboratory experiments showed that SO_2 is completely reduced at 600°C to H_2S. The elemental sulphur is completely absent from the reduction products. The reaction is described as follows:

$$3\ H_2 + SO_2 = 2H_2O + H_2S \quad (1)$$

- **Chemisorption of sulphur**

Sulphur chemisorption and carbide formation occur simultaneously. Sulphur has a highly active surface. It tends to be strongly absorbed or segregated at the surfaces of catalytic iron and Fe3C particles. The reaction is described as:

$$H_2S = H_2 + S_{ads} \quad (2)$$

The reaction 2 leads to considerable coverage with adsorbed sulphur at low sulphur activities as [42].

$$As = Ks\ .\ pH_2S/pH_2\ ,\ \text{with Ks: equilibrium constant}$$

The micrographs (Fig.11 and Fig.12) show a very thin FeS layer. Laboratory experiments indicate that this FeS layer is formed immediately when the gas SO_2 is injected.

- **Formation of Fe_3C and Fe_5C_2 Hägg iron carbides**

As shown in Figures 6 and 10, for the samples exposed to a low SO_2 content (0-10-50 ppm), PXRD patterns and TEM images revealed the large presence of Fe_3C but also the formation of sp2 carbon. In those cases, Fe_5C_2 iron carbides are not formed.
For an exposition at higher contents (50 - 100 - 1000 ppm), the carbon formation strongly decreases and the presence of Fe_5C_2 is observed.
The formation of the Hägg carbide (71.4 at. % Fe) would be explained by the partial depletion of iron in the cementite phase (75 at. % Fe) according to the reaction:
$2\ Fe_3C + S_{adsorbed} \rightarrow Fe_5C_2 + FeS$
In a paper about the influence of H_2S on metal dusting [40], Schneider *et al.* also reported the same experimental results. These authors observed the formation of cementite Fe_3C at low contents of H_2S and the formation of the Hägg carbide Fe_5C_2 at higher contents of H_2S.

- **Inhibition of the carbon deposition catalysed by Fe_3C (from the reduction of Fe_2O_3) in presence of H_2.**

The literature about metal dusting corrosion indicates that the addition of sulphur compounds (H_2S) in the atmosphere inhibits metal dusting and prevents the cementite decomposition [23]. The formation of the FeS layer limits the decomposition of the metastable cementite: Fe3C ➔ 3 Fe + C and the carbon nucleation. The adsorbed big sulphur S^{2-} ions block the reaction sites for the carburization reactions and the carbon transfer can occur only on sulfur free areas (1- θs), where θ_S is the fractional occupancy of the S adsorption sites.
TEM-EDS analysis revealed the formation of an iron sulphide inner layer (0.5-1 nm), surrounding the iron carbide nanoparticles (Fig. 11 and Fig.12). The iron provided to form the inner FeS layer is coming from the cementite (Fe_3C).
The protective layer of FeS has another beneficial effect. As shown previously [15], the nanometre size and the specific surface of catalytic particles promote the growth of carbon fibres.

FeS acts as a H_2-CO barrier and limits the reaction of iron oxide reduction by H_2 and CO, the phase transformation and recrystallisation that leads to volumetric change and the increasing of the iron carbide specific area, as shown in Figure 9.

In principle, sp^2 carbon nucleation and growth should be prevented by this monolayer FeS on the catalytic surface. But the FeS layer is not stable, S adsorption is a dynamic phenomenon and there are always some defects and vacancies in the FeS monolayer which will lead to a slow continued carbon formation. Thus, sulphur strongly retards but not fully suppress carbon formation. This explains a linear carbon growth rate of 0.3 $mg.h^{-1}$ for 1000 ppm SO_2 (see Fig.5 and table 3) and the outer layer surrounded the iron carbide particles (Figures 11 and 12). The STEM-EDS analysis revealed no sulphur but a significant amount of carbon, iron and oxygen in the outer layer. The mechanism explaining the formation of this layer remains an open question that it would be worth to study in detail for a publication in a subsequent paper. Figure 13-b summarizes the mechanism of carbon inhibition produced the Boudouard reaction by adjunction of sulphurous species.

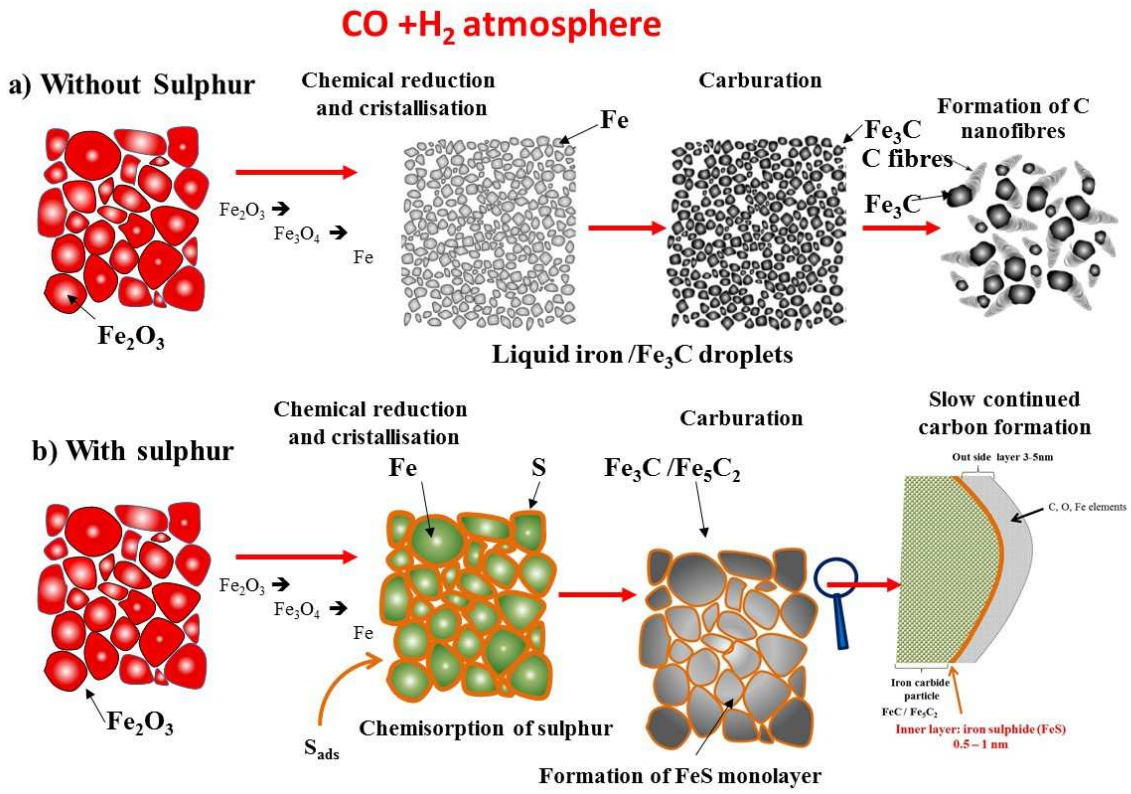

Figure 13- The formation of carbon from the Boudouard reaction, under CO/H_2 gas, catalysed by iron oxide particles a) without sulphur addition and b) with sulphur addition

5. Practical application to CO/H_2 resistant refractories

The retarding effect of sulphur on the carbon deposition produced by the Boudouard reaction by gaseous sulphur has been validated by an industrial refractory material (low cement castable: Refracast LCC-80R/TS – Refratechnic). Its chemical composition is given in Table 4.

Table 4- Chemical composition of the low cement castable [a]

Oxides	wt. %
Al_2O_3	81
SiO_2	16
CaO	2.5
Fe_2O_3	0.5

[a] Data as provided by Refratechnic company

This castable, doped with 5 wt.% of iron oxide particles to enhance the carbon deposit, was dried and pre-fired in air at 900 °C, for 8 hours. Two experiments were carried out:

- Experiment 1. The samples were heated to 600°C under Ar, at a rate of 10°C min^{-1} prior to being exposed to the CO/H_2 gas with a 28 L.h-1 flow rate, for 3 hours.
- Experiment 2. The samples were heated to 600°C under air prior to being exposed to the CO/H_2 gas containing 100 ppm of SO_2 (g).

The results are presented in figure 14.

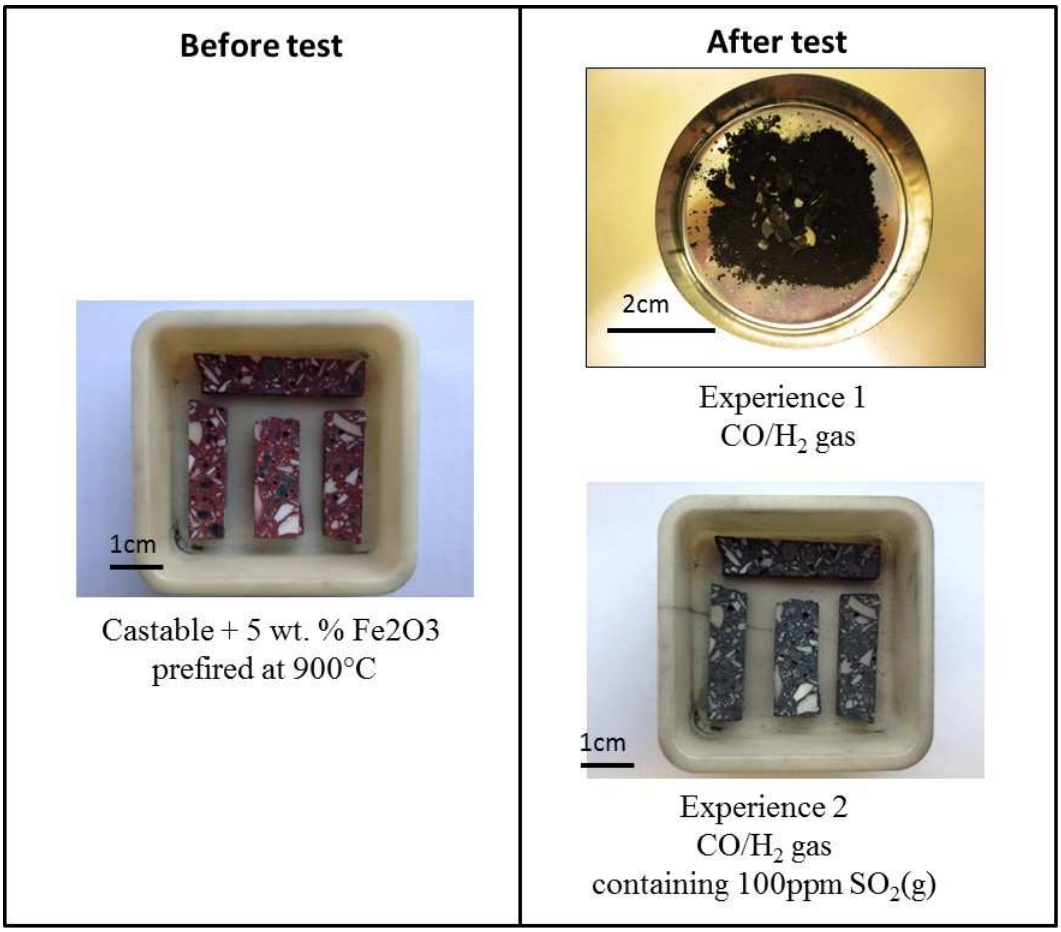

Figure 14. Photography of refractory samples before and after exposure to CO/H_2 and CO/H_2 containing 100 ppm of $SO_2(g)$

The samples exposed to CO / H_2 gas are much damaged and an important carbon deposit is observed. The samples exposed to CO / H_2 containing 100 ppm of SO_2 (g) are not damaged. There is no significant carbon deposit.

This work reveals that the addition of sulphurous gas (100ppm) in CO / H_2 gas in an effective solution and an efficient inhibitor to limit the carbon formation and the damage of refractories. For a specific industrial application, it will be essential to ensure that

- The processed materials are not contaminated with sulphur
- Sulphur release is compatible with environmental problems
- The temperatures of the refractory lining do not allow the condensation of sulphuric acid in colder parts.

This is the case with the future low CO-blast furnaces.

- The addition of SO_2 into CO-H_2 gas is very weak (100 ppm)
- The processed materials (elaboration of pig iron) allow low contamination with sulphur.

- The blast furnace gas is purified or its reuse (valorization as energetic gas) is possible.

It's obvious as well, that the addition of a sulphur carrier to the refractory raw material mix is not a practical solution, because the FeS-layer is not stable, as described in this paper.

6. Conclusions

The inhibition of the carbon formed by the Boudouard reaction and catalysed by Fe_3C has been investigated under the most favourable conditions of the reaction, i.e., in the presence of H_2 at 600 °C. This work reveals that sulphur, in the solid and gaseous states, is an efficient inhibitor to limit the carbon formation. From 100 ppm of $SO_2(g)$, the carbon growth rate decreases by a factor of 70 compared to an experiment without inhibitor, but the reaction is not completely prevented. In a CO/H_2 mixture at 600 °C, iron oxide particles are chemically reduced to Fe_3C and their sizes decrease. With the addition of sulphur such as 100 to 1000 ppm of $SO_{2(g)}$, the size of iron oxide particles (Fe_2O_3) decreases to a lesser extent but are still reduced to cementite (Fe_3C) and to Hägg iron carbide (Fe_5C_2). The sulphur intake has contributed to the formation of a very thin FeS layer (0.5 – 1 nm) around the iron carbide particles, preventing the catalytic effect of the Boudouard reaction.

Sulphur has a retarding effect. However, a temporary exposition of SO_2 (1000 ppm) has a lesser effect compared to a continuous exposition of SO_2 (100 ppm).

This study associated with the previous work [15], [16], shows that is possible to control the structure, size and organisation of the sp^2 carbons produced by the Boudouard reaction, catalysed by iron oxides.

- In the presence of pure CO gas, a carbon with a high structural organisation and an important coherent domain diameter is produced in the form of shells around the catalyst particles;
- In the presence of a CO and H_2 mixture, a carbon with a nanofibre morphology is favoured;
- In the presence of CO and H_2 mixture with an addition of S, the catalytic effect of the iron oxide particles is prevented.

This study paves the way to an effective solution to limit the sp^2 carbon deposition by the Boudouard reaction catalysed by iron oxides in the presence of hydrogen by poisoning the Fe_3C catalyst with sulphur.

Acknowledgements

This research was supported by the French National Agency: ADEME (TGRBF project).
The authors acknowledge the ICMN laboratory (Orléans, France) for the CM20 TEM access and the GENESIS platform for the TEM JEOL ARM 200F access. GENESIS is supported by the Région Haute-Normandie, the Métropole Rouen Normandie, the CNRS via LABEX EMC and the French National Research Agency as a part of the programme "Investissements d'avenir" with the reference ANR-11-EQPX-0020.
Annie Richard and Dr Ahmed Bachar are also acknowledged for the SEM/EDS analysis and for preliminary tests.

References

[1] Boudouard O. Les phénomènes de combustion dans les foyers industriels. Rev. Phys. Chim. Appl. Ind. 1901; 25: 385-91.

[2] Turkdogan E, Vinters J. Catalytic effect of iron on decomposition of carbon monoxide: I. Carbon deposition in H_2-CO mixtures. Metallurgical Transactions 1974; 5:11-19.

[3] Walker P, Raicszawski J, Imperial G. Carbon Formation from Carbon Monoxide-Hydrogen Mixtures over Iron Catalysts. I. Properties of Carbon Formed., II. Rates of carbon formation. J. Phys. Chem. 1959; 63: 133-149

[4] Baird T, Fryer J, Grant B. Carbon formation on iron and nickel foils by hydrocarbon pyrolysis—reactions at 700°C. Carbon 1974; 12(5): 591-602.

[5] Chizikov D. Dokl. Akad. Nauk. S.S.S.R. 1957;115: 586.

[6] Hughes E, Thomas J. Fuel 1962; 41: 297.

[7] Irving S, Walker P. Interaction of evaporated carbon with heated metal substrates. Carbon 1967; 5(4): 399-400.

[8] Robertson S. Carbon formation from methane pyrolysis over some transition metal Surfaces -I. Nature and properties of the carbons formed. Carbon 1970; 8(3): 365-368.

[9] Banerjee B, Hirt T, Walker P. Pyrolytic Carbon Formation from Carbon Suboxide. Nature 1961; 192: 450-451.

[10] Presland A, Walker P. Growth of single-crystal graphite by pyrolysis of acetylene over

metals. Carbon 1969; 7(1):1-4

[11] Ruston W, Warzee M, Hennaut J, Waty J. The solid reaction products of the catalytic decomposition of carbon monoxide on iron at 550°C. Carbon 1969;7(1): 47-57.

[12] Nolan P, Lynch D, Cutler A. Catalytic disproportionation of CO in the absence of hydrogen: encapsulating shell carbon formation. Carbon 1994; 32(3):477-483.

[13] Dai H, Rinzler A, Nikolaev P, Thess A, Colbert D, Smalley R. Single-wall nanotubes produced by metal-catalyzed disproportionation of carbon monoxide. Chemical Physics Letters 1996; 260: 471-475.

[14] Krause O, Pötsche J. The predictability of CO resistance of refractory materials by state-of-the-art test methods-a technical and scientific approach, Interceram 2008; 57:176-180.

[15] Bost N, Ammar M, Bouchetou M L, Poirier J. The catalytic effect of iron oxides on the formation of Nano-carbon by the Boudouard reaction in Refractories. Journal of the European Ceramic Society 2016; 36:2133-2142.

[16] Bost N, Canizarès A, Ammar M, Raimboux N, Melin P, Simon P, Poirier J. Probing the structural organisation of sp2 carbons obtained by the Boudouard reaction using in situ Raman scattering in reducing conditions. Vibrational Spectroscopy 2016; 87:157-163.

[17] Ruoff R, Lorents D. Mechanical and thermal properties of carbon nanotubes. Carbon 1995;33(7) : 925-930.

[18] Yazdanbakhsh A, Grasley Z, Tyson B, Al-Rub R. Challenges and Benefits of Utilizing Carbon Nanofilaments in Cementitious Materials. Journal of Nanomaterials 2012; 2012:1-8.

[19] Drzal L, Fukushima H. Conference Proceedings of High Performance Fillers, paper 15, 2006.

[20] Grabke H J. Thermodynamics, mechanisms and kinetics of metal dusting. Materials and Corrosion 1998; vol. 49 [5]:303-308.

[21] Zeng Z, Natesan K. Relationship between the Growth of Carbon Nanofilaments and Metal Dusting Corrosion. Chemistry of Materials 2005; 17 (14):3794-3801.

[22] Chu C M, Mumford J D, Ramanarayanan T.A. Mechanisms of Metal Dusting. Corrosion of Iron Journal of the Electrochemical Society 2002; 149 (7):348-355.

[23] Grabke H, R. Krajak R, Paz J. On the mechanism of catastrophic carburization: metal dusting. Corrosion Science 1993; 35:1141-1150.

[24] Schneider A, Inden G, Grabke H, Wei Q, Pippel E, Woltersdorf J. Effect of H_2S on

formation and decomposition of Fe_3C and Fe_5C_2 under metal dusting conditions. Steel Research 2000;71: 179-184.

[25] Ermakova M, Ermakov D, Chuvilin A, Kuvshinov G. Decomposition of Methane over Iron Catalysts at the Range of Moderate Temperatures: The Influence of Structure of the Catalytic Systems and the Reaction Conditions on the Yield of Carbon and Morphology of Carbon Filaments. Journal of Catalysis 2001;201:187-197.

[26] Berry T, Ames R, Snow R. Influence of impurities and role of iron carbides in deposition of carbon from CO. Journal of the American Ceramic Society 1956; 39: 308-318.

[27] Schneider A, Inden G. Computer Coupling of Phase Diagrams and Thermochemistry 2007; 31:141-147.

[28] Schneider A, Grabke H. Effect of H_2S on metal dusting of iron. Materials and Corrosion 2003; 54(10):793-798.

[29] Karcher W, Glaude P. Inhibition of carbon deposition on iron and steel surfaces. Carbon 1971; 9 (5):617-625

[30] Wood L, Vocadlo L, Knight K, Dobson D, Marshall W, Price G, Brodholt J. Thermal expansion and crystal structure of cementite, Fe_3C, between 4 and 600 K Determined by time-of-flight neutron powder diffraction. Journal of Applied Crystallography 2004; 37:82-90.

[31] Leineweber A, Shang S, Liu Z, Widenmeyer M, Niewa R. Crystal structure determination of Hägg carbide, x-Fe_5C_2 by first-principles calculations and Rietveld refinement. Zeitschrift für Kristallographie 2012; 227(4):207-220.

[32] Ammar M R, Galy N, Rouzaud J N, Toulhoat N, Vaudey C E, Simon P, Moncoffre N. Characterizing various types of defects in nuclear graphite using Raman scattering: Heat treatment, ion irradiation and polishing. Carbon 2015; 95 :364–373.

[33] Ammar MR, Rouzaud J N. How to obtain a reliable structural characterization of polished graphitized carbons by Raman micro spectroscopy. Journal of Raman Spectroscopy 2011; 43(2): 207-211.

[34] Maslova O A, Ammar M R, Guimbretière G, Rouzaud J N, Simon P. Determination of crystallite size in polished graphitized carbon by Raman spectroscopy, Physic ReviewB- Condens Matter MaterPhys 2012; 86(13):13425.

[35] Pimenta M A, Dresselhaus G, Dresselhaus M S, Cançado L G,Jorio A, Saito R. Studying disorder in graphite-based systems by Raman spectroscopy Phys. Chem. Chem. Phys.2007. 9:1276-1290.

[36] M. Nakamizo M, H. Honda H, M.I. Nagaki M I. Raman spectra of ground natural graphite. Carbon 1978; 16: 281-283

[37] F. Negri F, E. Di Donato E, M. Tommasini M, C. Castiglioni C, G. Zerbi G, K. Mullen K, Resonance Raman contribution to the D band of carbon materials: modeling defects with quantum chemistry. J. Chem Phys.2004;120(24) :11889 – 11900.

[38] Castiglioni C, Tommasini M, Zerbi G. Raman spectroscopy of polyconjugated molecules and materials: confinement effect in one and two dimensions. Philos. Trans. R. Soc. London Ser. A – Math. Phys. Eng. Sci. 2004 ; 362: 2425– 2459.

[39] Donazzi A, D. Pagani D, A. Lucotti A, M. Tommasini M, A. Beretta A, G. Groppi G, Castiglioni C, Forzatti P. Annular reactor testing and Raman surface characterization in the CPO of methane and propyleneAppl. Catal. A: Gen. vol 2014; 474:149–158.

[40] Schneider A,Viefhaus H,Inden G, Grabke H,Müller-Lorenz E. Influence of H_2S on metal dusting. Materials and Corrosion 1998; 49(7):336-339.

[41] Feng T, Huo M, Zhao X, Wang T, Xia X, Ma C. Reduction of SO_2 to elemental sulfur with H_2 and mixed H_2/CO gas in an activated carbon bed. Chemical Engineering Research and Design 2017;121: 191-199.

[42] Grabke H. J., Moszynski D.,E. M. Müller-Lorenz E.M.,Schneider A. Role of sulphur in carburization, carbide formation and metal dusting of iron. Surface and interface analysis 2002;34: 369-374.